International Conference on Space Optics—ICSO 2006

Noordwijk, Netherlands

27–30 June 2006

Edited by Errico Armandillo, Josiane Costeraste, and Nikos Karafolas

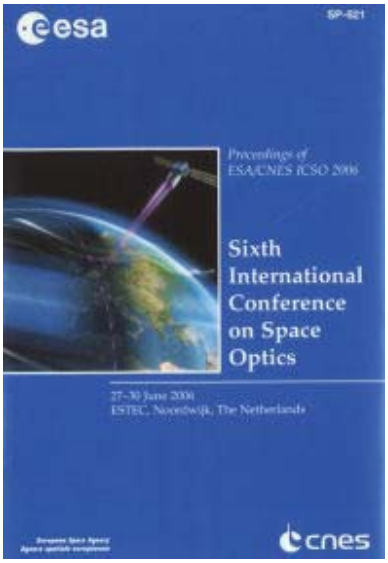

In-flight calibration of the ozone monitoring instrument

Ruud Dirksen, Marcel Dobber, Robert Voors, Quintus Kleipool, et al.

International Conference on Space Optics — ICSO 2006, edited by Errico Armandillo, Josiane Costeraste, Nikos Karafolas, Proc. of SPIE Vol. 10567, 1056724 · © 2006 ESA and CNES
CCC code: 0277-786X/17/$18 · doi: 10.1117/12.2308149

IN-FLIGHT CALIBRATION OF THE OZONE MONITORING INSTRUMENT

Ruud Dirksen[1,2], Marcel Dobber[1], Robert Voors[1], Quintus Kleipool[1], Gijsbertus van den Oord[1], Pieternel Levelt[1]

[1]Royal Netherlands Meteorological Institute, Wilhelminalaan 10, 3732 GK De Bilt, The Netherlands, dirksen@knmi.nl
[2]Space Research Organization of The Netherlands, Sorbonnelaan 2, 3584 CA Utrecht, The Netherlands, dirksen@sron.nl

ABSTRACT

This paper discusses various aspects of the on-ground and in-flight calibration of the OMI instrument.

1. INTRODUCTION

The Ozone Monitoring Instrument (OMI) is part of NASA's EOS-AURA mission that was launched on July 15 2004. The mission objectives concern the recovery of the ozone layer, ozone depletion at the poles and tropospheric air-pollution [1].
OMI is a nadir viewing, UV-VIS imaging spectrometer that observes in a 700km altitude sun-synchronous polar orbit the back-scattered light from the Earth's atmosphere in the 270-500nm wavelength range with a typical resolution of 0.5nm. Its wide field of view of 115 degrees yields a 2600km wide swath that enables global daily coverage at the equator. The unprecedented high spatial resolution of OMI (24x13km^2 ground pixel size) improves the accuracy of the data products because of the higher change of observing cloud-free pixels and it also allows for detection and monitoring of air pollution on an urban scale. Another novelty for this kind of Earth observing instruments is the use of 2D frame transfer CCD detectors that allow for simultaneous recording of the spatial and the spectral dimension. This removes the need for a scan mirror and enables continuous scanning of the scene without data gaps.
The data products of OMI include total column measurements of ozone, nitrogen dioxide, sulfur dioxide and other atmospheric trace gases as well as ozone profile, clouds and aerosols. The total column amounts of ozone, NO_2 and other atmospheric constituents are determined using the DOAS technique [2]. For OMI the retrievals are based on comparing the measured Sun-normalized Earth radiance to a high-resolution literature absorption cross-section that has been convolved with the instrument spectral slitfunction [3]. The spectral slitfunction has been calibrated with great accuracy using a novel technique employing an echelle grating [4]. This method and the results are discussed in section 3. Diffuser spectral features are discussed in section 4, the viewing properties and geolocation validation are discussed in section 5, and section 6 discusses straylight calibration.

2. INSTRUMENT DESCRIPTION

The OMI instrument consists of a telescope with a 115° field of view which images the incident light on the entrance slit of the spectrometer. The length of the entrance slit (44 mm) corresponds to the viewing dimension perpendicular to the flight direction. The width of the entrance slit (300μm) defines the 1-degree field of view in the flight direction, which corresponds to approximately 10km on the surface of the Earth. The 2 seconds integration time of the detectors sets the length of the ground pixels in the flight direction to 13km. The wavelength range is divided into two separate channels, the UV channel (270-380nm) and the Visible channel (350-500nm). Each spectral channel is equipped with its own 2D CCD detector measuring 780 pixels (spectral dimension) by 576 rows (viewing dimension). The UV channel is divided into two sub-channels, UVI (270-311nm) and UVII (307-380nm) that are imaged on different areas of the same CCD detector. This has been done to reduce the straylight from higher wavelengths and to optimize the settings for the wavelengths below 310 nm, as in this wavelength range the Earth radiance decreases by three to four orders of magnitude because of the strong absorption by ozone in the Hartley-Huggins band. Furthermore the spatial dimension of the channel has been compressed by a factor two to improve the signal-to-noise. In the nominal operational mode 8 rows are binned during readout, which results in images of 60 binned rows for UVII & VIS and 30 binned rows for UVI. This yields a ground pixel size of 24x13km^2 for the nadir pixels in UVII and VIS, in UVI this pixel is twice as large in the swath direction, 13x48km^2. The spectral resolution and spectral sampling of the channels are listed in table 1.

Channel	Range (nm)	Resolution (nm)	Sampling (nm/pixel)
UVI	264-311	0.63	0.33
UVII	307-383	0.42	0.14
VIS	349-504	0.63	0.21

Table 1. Overview of the spectral properties of OMI

Proc. '6th Internat. Conf. on Space Optics', ESTEC, Noordwijk, The Netherlands, 27-30 June 2006 (ESA SP-621, June 2006)

For observing the solar irradiance spectrum the instrument is equipped with three on-board reflection diffusers. Two ground aluminum diffusers and one ground quartz diffuser. The aluminum diffusers are used once per week and once per month respectively to track the radiometric stability. The quartz diffuser is used every day to provide the solar reference spectrum to derive the Sun-normalized Earth radiances which are input for the level 2 retrieval algorithms. The reason for using the quartz diffuser is that it has smaller spectral features than the aluminum diffusers; this topic is discussed further in section 4. Besides the reflection diffusers OMI is also equipped with a transmission diffuser that is used in cooperation with the on-board white light source, to monitor instrument stability and detector calibration. During the on-ground performance and calibration measurements there was the possibility to illuminate the transmission diffuser via the calibration port, an additional piece of optics that coupled the light into the instrument. When the on-board diffusers are employed the entire entrance slit of the spectrograph is illuminated. Save for the primary telescope mirror the path through the instrument is identical for light emerging from the diffusers and for light entering the instrument via the radiance port.
For a more detailed description of the instruments design and operation the reader is referred to [6].

3. SPECTRAL SLITFUNCTION

The spectral slitfunction determines how a monochromatic spectral line is imaged on the detector. In fact the slitfunction describes how an input spectrum is smeared in the spectral domain and how its shape is recorded by the instrument. The slitfunction defines the instruments spectral resolution.
In case of DOAS-based retrieval techniques the shape and magnitude of spectral features induced by absorption by trace gases in the reflectance spectrum of the Earth's atmosphere are fitted. In order for the retrieval algorithms to work properly and to obtain reliable column densities requires knowledge of the shape of the absorption spectrum as recorded by the OMI instrument. This can be achieved by recording the absorption spectra of the trace gases of interest with the instrument in a laboratory set-up, or by accurately measuring the spectral slitfunction and use these results to convolve high resolution absorption cross section spectra from literature. For the OMI project the choice was made to accurately calibrate the spectral slitfunction for all wavelengths and viewing angles. Beside for the DOAS-based retrievals the spectral slitfunction is also used in the in-flight spectral calibration as the latter is based on fitting the positions of the Solar Fraunhofer lines. The spectral properties listed in table 1 show that the ratio spectral resolution/spectral sampling equals three for UVII and VIS, and 1.7 for UVI. The low sampling of the spectral resolution is too coarse to retrieve an accurate calibration of the spectral slitfunction from e.g. the measurement of a spectral line source. In this case a light source with wavelength-tunable spectral lines is needed to overcome the limited spectral sampling. Such a light source was developed and used to calibrate OMI's spectral slitfunction during the on-ground calibration campaign. This new-designed optical stimulus employs an echelle grating to produce an output beam containing many well-separated spectrally narrow peaks. Changing the illumination geometry of the grating (i.e. turning the echelle grating) changes the positions of the peaks. A more detailed description of the design of the echelle based optical stimulus, the analysis of the measurement data and the results is given in [4].

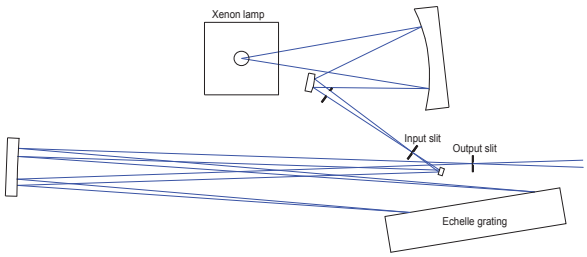

Fig. 1. Schematic layout of the echelle optical stimulus used to calibrate the OMI spectral slitfunction.

The echelle stimulus works as follows: an echelle grating is illuminated by a collimated beam of white light near grazing incidence. The illumination geometry, the angles of incidence and diffraction, are defined by the entrance and exit slits, a schematic layout of the optical stimulus is shown in figure 1. In this configuration the exit beam is degenerate, meaning that it contains many diffraction orders. The wavelengths of the orders in the output beam are given by the grating formula

$$d(\sin\theta_i + \sin\theta_d) = m\lambda \qquad (1)$$

with d the grating constant of 1.39 x 10^{-5} m, θ_i and θ_d the angles of incidence and diffraction, λ the vacuum wavelength and m the diffraction order. The diffraction order peaks are 0.03-0.05nm wide (depending on the wavelength), which is well below the spectral resolution of the OMI instrument and the peak separation ranges from 2.7 nm at 270nm to 9nm at 500 nm. By turning the Echelle grating that is mounted on a rotation table the angles θ_i and θ_d change which causes the diffraction orders to move in wavelength space. By monitoring the response of a detector pixel to a passing diffraction order the spectral slitfunction is retrieved. Some data processing still is necessary to correct for the stimulus straylight and for the grating efficiency that varies with θ_i and θ_d. The output beam of the

echelle stimulus was coupled into the instrument via the calibration port so that it illuminates the internal transmission diffuser.
By using the transmission diffuser the full length of the spectrograph entrance slit is illuminated so that the slitfunction can be determined for all viewing angles in a single measurement run. The transmission diffuser also ensures that the width of the entrance slit is illuminated homogeneously, this is important because the slitfunction is the monochromatic image of the entrance slit on the detector and inhomogeneous illumination of the entrance slit affects the measured slitfunction profile.
Using this setup the slitfunction profile was measured for each CCD row over the full OMI wavelength range with a sampling that is about ten times higher than the instruments sampling, which is demonstrated in figure 2. The retrieved slitfunction profiles were fitted by the following analytical function

$$A_0 e^{-\left(\frac{x-x_0}{w_0}\right)^2} + A_1 e^{-\left(\frac{x-x_1}{w_1}\right)^4} \qquad (2)$$

with A_0, x_0 and w_0 the amplitude, central position and width of the first term respectively. Idem for A_1, x_1 and w_1 in the second term. This function is the combination of a Gaussian profile and a broadened flat-topped term. The Gaussian term suffices to fit the slitfunction profiles in the UVI channel, but for accurate fitting of the profile in UVII and VIS the second term of equation 2 is necessary.

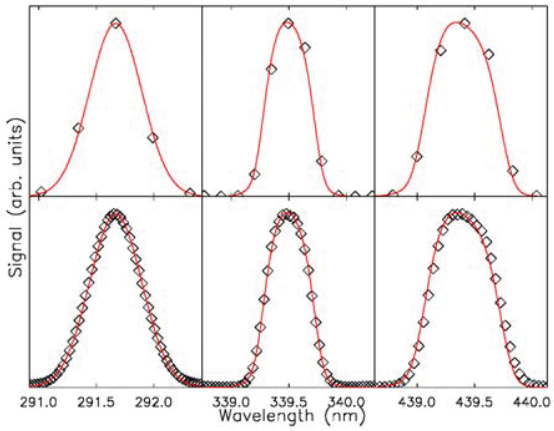

Fig 2. The shape of the spectral slitfunction in UVI (left column), UVII (middle column) and VIS (right column). The plots in the upper row present a spectral line recorded by OMI, revealing the limited sampling. The plots in the bottom row show for the same wavelengths the slitfunction measured using the Echelle stimulus. The red traces represent fits to the profiles of the lower plots.

The function of equation 2 adequately parameterizes the asymmetry of the slitfunction profile in the VIS channel by means of the central position parameters x_0 and x_1.
The comparison between the absorption spectrum of NO_2 measured by OMI in a laboratory gas cell setup and a high resolution absorption cross section spectrum from literature convolved with the OMI slitfunction showed residual differences with an rms. value of 0.4% [5]. Furthermore the convolved high resolution literature cross section spectra were used to retrieve reliable NO_2 concentrations from zenith sky measurements performed with the OMI instrument. [5]. These findings confirm that the spectral slitfunction has been calibrated accurately and that the approach in the OMI project to invest in accurately calibrating the slitfunction and using absorption cross section spectra from literature instead of performing extensive gas cell measurements is valid. Another test of the accuracy of the spectral slitfunction is to compare the OMI measured solar irradiance spectrum to a high-resolution reference solar spectrum convolved with the OMI slitfunction. The result of this comparison is shown in figure 3, where the residuals are plotted versus wavelength for all three spectral channels.

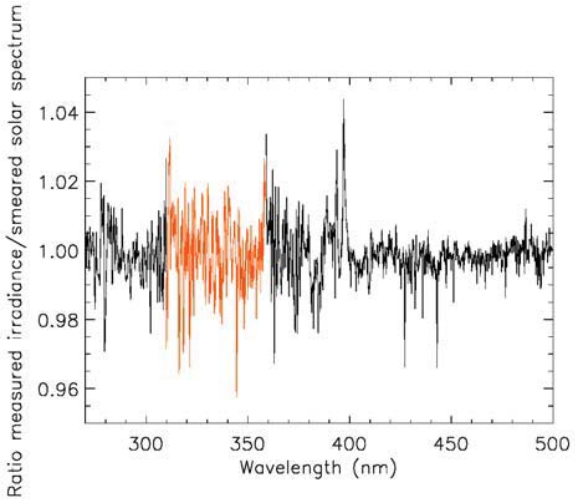

Fig. 3. Comparison between an OMI solar irradiance measurement and a high-resolution solar spectrum convolved with the OMI spectral slitfunction. The red trace represents the residual for UVII, the black traces represent the residuals for UVI and VIS.

The residuals are well below 2% in UVI and VIS, though they are a bit larger in UVII. The residuals are mainly attributed to inaccuracies in the slitfunction parameterization and to inaccuracies in the solar reference spectrum. However the residuals being this small is a promising result. Two features that clearly stand out in the residuals haven't been discussed yet, these are the features connected to the MgII and CaII Fraunhofer lines near 290nm and near 396nm respectively. The occurrence of these strong features in

the residuals is attributed to changes in the solar activity, which is known to have a considerable effect on the depth of these absorption lines.

4. DIFFUSER SPECTRAL FEATURES

The on-board reflection diffusers that are used for the solar irradiance measurements exhibit spectral features. These spectral features are caused by interference from remaining regular structures on the roughened (ground) surface of the diffuser. Via their presence in the solar irradiance spectrum these features show up in the Sun normalized Earth radiance spectrum. When the diffuser spectral features resemble the absorption features of atmospheric trace gases they will affect the DOAS-based retrieval of these trace gases as the DOAS retrievals fit the absorption structures in the Earth's reflectance spectrum. DOAS retrievals are very sensitive to spectral artifacts such as diffuser features. In order not to interfere with the DOAS retrievals the diffuser features should be smaller than 10^{-4}. As mentioned in the instrument description, OMI has three on-board reflection diffusers for solar irradiance measurements, two ground aluminum diffusers and one quartz volume diffuser. The aluminum diffusers exhibit features with peak-peak amplitudes of several percent, which is well above the required level. The quartz volume diffuser (QVD) exhibits spectral features that are considerably smaller; for this reason the QVD is used for the daily solar irradiance measurements to provide the solar reference spectrum, which is used to calculate the Earth reflectance spectrum. The QVD is a new-developed diffuser that consists of a quartz plate with two ground surfaces and the lower surface is covered with a reflective aluminum coating. Therefore light that hits the diffuser is scattered by the upper surface, travels through the quartz to be scattered and reflected by the lower surface and finally is scattered again by the upper surface and leaves the diffuser. As a result the light is scattered by three surfaces when reflecting from the diffuser, which effectively renders it a volume diffuser, and this considerably reduces the spectral features.

The diffuser spectral features are not visible directly in the solar irradiance spectrum because these are much smaller than other spectral features like the solar Fraunhofer lines, but they can very well be visualized by taking the ratio of two solar irradiance measurements taken at different illumination angles. This stems from the fact that the features are caused by interference effects: their position and magnitude change with varying illumination (azimuth and elevation) angle. The latter can be used to our advantage: during a solar irradiance measurement typically 77 images are recorded while the elevation angle changes from –4° to +4°. By averaging the images with elevation angles between [–3°,+3°] the diffuser features are smeared and partly cancel, yielding an averaged irradiance image with smaller diffuser features. Furthermore, averaging improves the signal-to-noise of the spectrum.

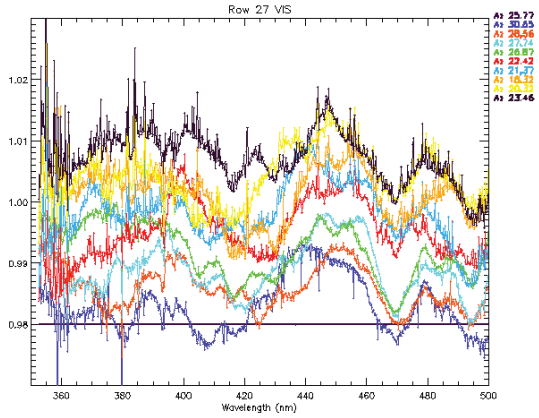

Figure 4. Elevation averaged solar irradiance measurements at various azimuth angles divided by the averaged measurement at 25.77° azimuth angle. Data taken from the VIS channel for one of the aluminum diffusers.

As can be seen in figures 4 and 5, the spectral features of the quartz volume diffuser are about a factor 10 smaller than the spectral features generated by the aluminum diffuser. The plots were produced using in-flight measurements. Note the different y-axis scale for both figures.

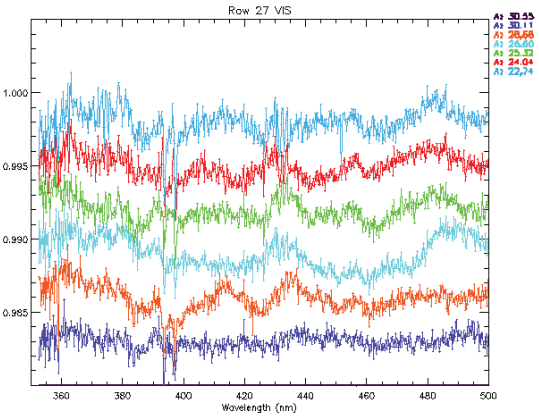

Figure 5. Same as figure 4 but now for the QVD diffuser. Note the different y-axis scale.

The diffuser features were partly characterized during the on-ground calibration but the resulting dataset had too coarse sampling of the azimuth and elevation angles to be used for calibrating the effect. As a result the diffuser features are not corrected for in the level 1 solar irradiance product, which is not absolutely

necessary in view of the measures that were taken to reduce the features.
These measures are:

- using the QVD diffuser
- elevation averaging
- binning of rows (another form of averaging)

After more than one and a half year of operation there is a vast amount of in-flight solar irradiance data available. This dataset has superior sampling of both the elevation and the azimuth angles in comparison with the on-ground measured data. This dataset will be used to study and characterize the spectral features in more detail.
One of the reasons for the diffuser features being this large is the fact that the diffusers are located close to the focus of the telescope so that the projection of the instantaneous field of view of a detector pixel on the diffuser covers a relatively small area (1-2 mm^2). This area is too small to cancel the interference effects from the diffuser surface.

5. GEO-LOCATION

The viewing properties of the OMI instrument were measured extensively during the on-ground calibration campaign, using a parallel with light beam entering the instrument through the nadir port. The optical stimulus produces a highly collimated beam with a 0.03° divergence, which corresponds to 0.1 unbinned pixel. The instrument was manipulated using a turn-tilt cradle to select the viewing swath angle, and by examining the signal for multiple pixel rows the pixel viewing direction was measured. Additionally the pixel field of view was measured by rotating the instrument and monitoring the response of a single CCD pixel.

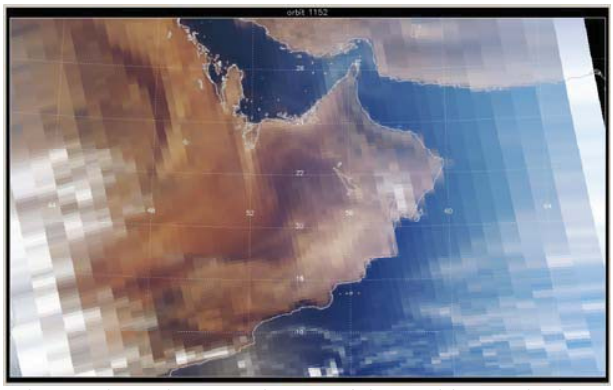

Fig 6. False color RGB-image of the Arabian penisula constructed from OMI level 1 data.

This is similar to the method of measuring the slitfunction as described in section 3 and yields its spatial equivalent: the spatial resolution. Because the turn-tilt cradle was not suitable to be used in vacuum conditions all viewing measurements were performed in ambient conditions. A number of measurements were taken to quantify the changes in viewing properties from ambient to flight representative vacuum conditions at 264K. These results were included in the viewing properties calibration parameters.
The viewing properties were validated by comparing geolocated level 1 data to known geographical features with high contrast, like coastal structures. For this purpose false color RGB images were created from the VIS channel data, an example of which is shown in figure 6. For the purpose of geolocation validation the instrument was operated for several days in the unbinned mode, which increases the cross track resolution at nadir approximately five times in comparison with the nominal binned mode. The results of these comparisons show that the geolocation in flight for various viewing angles is accurate to about 0.1 pixel, which corresponds roughly to 2km.

6. STRAYLIGHT

Straylight can be classified as either being spectral, light ending up at the wrong wavelength, or spatial, light ending up at the wrong viewing direction. Spectral straylight is especially important for wavelengths below 300nm where the Earth's radiance drops by several orders of magnitude because of absorption by ozone. In this case the straylight originating from higher wavelengths can easily exceed the useful signal at that wavelength. Spatial straylight is important for scenes with high contrast along the swath direction, for instance sea-ice transitions or clouds. In general spectral and spatial straylight are mixed meaning that light ends up at another wavelength and viewing location. The spectral straylight of OMI has been extensively calibrated using a beam of white light in combination with various bandpass and/or cut-on long-pass wavelength filters. The measurements were performed via the nadir port and via the calibration port. The spatial straylight was calibrated with measurements via the nadir port offering a beam of 2° to 3° divergence.
It was briefly discussed in section 2 how the optical design of OMI is optimized to reduce straylight below 300nm. The uncorrected measured spectral straylight fraction at 270nm is 8%, after correction the straylight contribution has decreased to approximately 1% of the signal at 270nm for uniform scenes. Analysis of in-flight radiance spectra reveals that for inhomogeneous cloudy scenes these clouds generate spectral straylight in UVI. This demonstrated by the plots of figure 7, the left panel shows the radiance signal at 320nm for all pixels in an orbit, the right panel shows the (straylight corrected) level 1 radiance signal at 280nm. In these plots the x-axis represents row number (swath angle) and the y-axis represents image number (flight

direction). The cloud structures that clearly show up at 320nm in the left panel should not be visible at 280nm because at this wavelength OMI can't look deep enough into the atmosphere to the altitudes where clouds reside. Instead of the rather homogenous image that one expects for 280nm, the right panel shows structures that correlate with the clouds in the left panel. The straylight features measure approximately 3% of the useful signal.

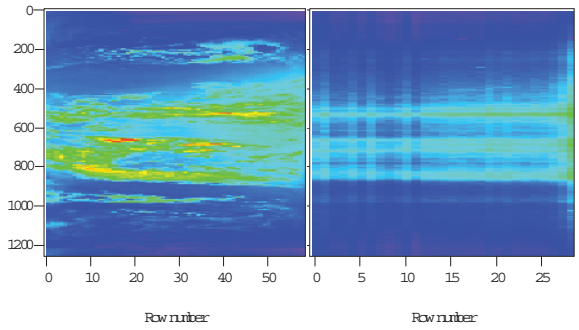

Fig. 7. Clouds introduce straylight features at 280nm. The left panel shows the level 1 radiances at 320nm, the right panel shows the level 1 radiances at 280m. The x-axis represents row number (swath direction), the y-axis respresents image number (flight direction).

The reason for this is the way that the dataprocessor corrects the spectral straylight. In the current implementation the straylight correction algorithm estimates the straylight in UVI based on the averaged signal level over all rows a wavelength band in UVII. This straylight estimate is subtracted from the entire UVI channel, neglecting row dependencies. In case of partly cloudy scenes this leads to an underestimation of the spectral straylight coming from clouds, resulting in residual cloud structures in UVI. A new correction algorithm that incorporates the row dependency of the straylight is being developed.

7. CONCLUSIONS

In this paper several topics of the calibration of the OMI instrument have been discussed. The OMI spectral slitfunction has been calibrated with high accuracy and sampling using a new method employing an echelle grating. In the OMI project the DOAS-based retrieval techniques use high resolution absorption cross section spectra from literature convolved with the OMI slitfunction. The comparison of an OMI measured solar irradiance spectrum with a high resolution solar reference spectrum convolved with the OMI slitfunction showed residuals smaller than 2%.
Diffuser spectral features can hamper DOAS-based retrievals of trace gas concentrations in the atmosphere. A new-developed quartz volume diffuser exhibits smaller features than the traditionally used aluminum diffusers. By using the QVD diffuser, by averaging over elevation angles and by binning of rows the size spectral features in the solar irradiance measurement has been reduced enough not to interfere with the DOAS retrievals. The spectral features of the aluminum and the QVD diffuser were investigated during the on-ground calibration campaign; the in-flight measurements will be used to further analyze and characterize the features.
The viewing properties OMI and the associated geolocation of the level 1 data has been validated by comparing with geographical structures. The geolocation is accurate to about 0.1 pixel which corresponds roughly to 2km.
The spectral straylight has been calibrated extensively during the on-ground calibration campaign and the straylight correction is capable of reducing the straylight contribution to 1% of the useful signal at 280nm for homogenous scenes. However partly clouded scenes introduces straylight features at this wavelength. A new correction algorithm that incorporates the row dependence of the straylight is being developed.

REFERENCES

1. Levelt P., et al., Science objectives of the Ozone Monitoring Instrument, *IEEE Trans. Geosc. Remote Sens.*, Vol. 44, 1199-1208, 2006.

2. Platt U., Differential Optical Absorption Spectroscopy (DOAS), *Air Monitoring by Spectroscopic Technique*, M.W. Sigrist, Ed., Wiley, New York, 1994.

3. Veefkind J.P., de Haan J.F., Brinksma E.J., Kroon M., Levelt P.F., Total Ozone from the Ozone Monitoring Instrument (OMI) using the DOAS technique, *IEEE Trans. Geosc. Remote Sens.*, Vol. 44, 1239-1244, 2006

4. Dirksen R., Dobber M., Voors R., Levelt P., Prelaunch characterization of the Ozone Monitoring Instrument transfer function in the spectral domain, to be published in *Applied Optics*, Vol. 45, 2006.

5. Dobber M., Dirksen R., Voors R., Mount G.H., Levelt P., Ground-based zenith sky abundances and in situ gas cross sections for ozone and nitrogen dioxide with the Earth Observing System Aura Ozone Monitoring Instrument, *Applied Optics*, Vol. 44, 2846-2856, 2005.

6. Dobber M.R., et al., Ozone Monitoring Instrument Calibration, *IEEE Trans. Geosc.Remote Sens.*, Vol. 44, 1209-1238, 2006.